Raman Spectroscopy Applied to Monitor Furfural Liquid-Phase Oxidation Catalyzed by Supported Gold Nanoparticles

Joëlle Thuriot-Roukos, Romaissa Khadraoui, Sébastien Paul, Robert Wojcieszak

ACS OMEGA

http://pubs.acs.org/journal/acsodf

Article

Raman Spectroscopy Applied to Monitor Furfural Liquid-Phase Oxidation Catalyzed by Supported Gold Nanoparticles

Joëlle Thuriot-Roukos,* Romaissa Khadraoui, Sébastien Paul, and Robert Wojcieszak

Cite This: *ACS Omega* 2020, 5, 14283−14290

Read Online

ACCESS | Metrics & More | Article Recommendations | Supporting Information

ABSTRACT: In this paper, Raman spectroscopy is used as a tool to study the mechanism of furfural oxidation using H_2O_2 as a reagent on gold nanoparticles (NPs) supported on hydrotalcites (HTs). This reaction was repeated, under the same conditions, but with different reaction times in a parallel multireactor system. The reaction media were analyzed using a macro device associated with a multipass cell permitting us to enhance the Raman signal by reflecting the laser beam 3 times. The Raman spectra showed the conversion of furfural to furoic acid without any chemical intermediates, thus privileging a direct pathway. Combining the results of the catalytic tests with those of the Raman study, the mechanism of furfural oxidation to furoic acid using gold NPs supported on HTs is proposed. The key points of this mechanism were found to be as follows: (i) the *in situ* formation of a base, originating from the Mg leaching from the HT support, initiates the oxidation of furfural by deprotonation; (ii) H_2O_2 used as a reagent in the solution increases the catalytic activity by its dissociation to form hydroxide ions; and (iii) the oxidation of furfural occurs on the surface of gold NPs and leads to higher furoic acid yield.

INTRODUCTION

Moving toward the development of greener technologies and reducing the carbon footprint of chemical industries imply the use of renewable biomass as a raw material to generate chemicals and biofuels.[1,2] In this context, the use of an appropriate catalyst is key to convert lignocellulosic biomass into biochemicals and fuels.[2] Furfural (furan-2-carbaldehyde) has been highlighted as one of the most promising renewable platform molecules.[2,3] Therefore, a variety of new catalytic processes have been developed for furfural transformation into high value-added molecules. Furoic acid (furan-2-carboxylic acid) is the first downline oxidation derivative of furfural. It is used in pharmaceutical, agrochemical, fragrance, and flavor industries.[3] Catalysts for the conversion of platform molecules obtained from biomass must be compliant with new processing conditions including an aqueous medium and a low-temperature reaction.[4] The most important challenge is to understand and obtain detailed information on the operating principles of solid catalysts in an aqueous phase. Raman spectroscopy is a powerful characterization technique that gives molecular information when used for investigating the reaction mechanism.[5] In contrast to infrared spectroscopy, Raman is less sensitive to changes in the dipole moment resulting in very weak signals from water. Thus, Raman can probe molecules having polarizable bonds in the aqueous phase.[6] The major drawback of Raman spectroscopy is its lack of sensitivity because of low Raman scattering but it can be enhanced using resonance Raman spectroscopy (RRS), surface-enhanced Raman spectroscopy (SERS), and coherent anti-Stokes Raman spectroscopy (CARS).[7,8] The combination of SERS and RRS techniques (*i.e.* surface-enhanced resonance Raman spectroscopy) can even increase the sensitivity up to 10 orders of magnitude when compared to conventional Raman spectroscopy.[7] Nevertheless, factors such as substrate instability or insufficient signal enhancement still limit the wide use of these techniques in the field of catalysis.[8] Another approach to study reaction mechanisms by Raman spectroscopy is to use fiber-optic probes. In this case, the Raman is usually coupled with other spectroscopic techniques such as IR and UV−vis.[9,10]

Attempting an *in situ* monitoring of a reaction medium containing a solid catalyst by Raman spectroscopy is usually unsuccessful. This failure is caused by the formation of bubbles when the heterogeneous reaction mixture has to be stirred or by strong fluorescence background (emanating from the solid catalyst), which obscures the Raman signal.[11]

In this paper, the high potential of using Raman spectroscopy to study the mechanism of an aqueous reaction using a powder catalyst is presented. To achieve that, a simple and convenient Raman optic device associated with a strategy of sampling was used. For the proof of concept, the selective oxidation of furfural to furoic acid was studied. For this reaction, the potential of hydrotalcite (HT) as a material for the catalyst support was explored. Noble metals were often found to be very efficient catalysts for oxidation reactions but gold-based catalysts have also been recently proved to be highly selective and stable.[12] To increase the catalytic activity and orientate the selectivity of the reaction, several studies have used H_2O_2 as an oxidant.[13,14] In this paper, the roles of

Received: January 8, 2020
Accepted: April 7, 2020
Published: June 9, 2020

https://dx.doi.org/10.1021/acsomega.0c00091
ACS Omega 2020, 5, 14283−14290

gold nanoparticles (NPs) supported on HTs as catalyst and of H_2O_2 used as a reagent are revealed based on a mechanistic study using the Raman spectra, inductively coupled plasma (ICP), and catalytic tests results.

RESULTS AND DISCUSSION

Catalyst Synthesis. HTs are composed of brucite-like layers in which a fraction of the divalent metal cations (*e.g.*, Mg^{2+}) coordinated octahedrally by hydroxyl groups has been replaced isomorphously by trivalent metal cations (*e.g.*, Al^{3+}), giving positively charged layers. The Mg/Al molar ratio can be tuned changing both the physical and chemical properties of the solid used as a support. The Mg/Al molar ratio was set to (4:1; 2:1; 1:1; and 1:5) in order to prepare four supports with different acid−base properties. Then, 2 wt % of gold (Au) was deposited on each of the four supports.

Characterization of Catalysts. After synthesis, the catalysts were characterized by ICP in order to determine the chemical compositions of the materials (Mg, Al, and Au). The catalysts were named Au/HT-4:1, Au/HT-2:1, Au/HT-1:1, and Au/HT-1:5 according to the expected theoretical Mg/Al molar ratio as already mentioned. Table 1 gathers the ICP results.

Table 1. ICP Analysis Results

Mg/Al (molar ratio)	Mg/Al	Au wt %
HT-4:1	3.86 ± 0.19	1.64 ± 0.17
HT-2:1	1.75 ± 0.24	1.52 ± 0.55
HT-1:1	0.63 ± 0.06	1.83 ± 0.47
HT-1:5	0.15 ± 0.03	1.9 ± 0.38

The experimental Mg/Al ratios were found to be close to the expected values for a high Mg content (HT-4:1 and HT-2:1). In the case of the HT-1:1 support, the Mg content was much lower than the expected one (Table 1). As for HT-1:5, this support was designed to have the lowest content of Mg. Concerning gold, the amounts deposited on HT-1:1 (1.83 wt %) and HT-1:5 (1.9 wt %) were relatively higher than those deposited on HT-4:1 and HT-2:1 (1.64 and 1.52 wt %, respectively). Thus, the deposition of gold seems to depend on the acid−base properties of the support, as a higher quantity of gold was deposited on the less-basic sample (HT-1:1 and HT-1:5).

Figure 1 shows the transmission electron microscopy (TEM) image obtained for the Au/HT-4:1 sample. It can be clearly seen that gold NPs are highly dispersed on the surface with an average particle size of 3.5 nm (ranging between 2.5 and 5.5 nm counted from around 100 particles).

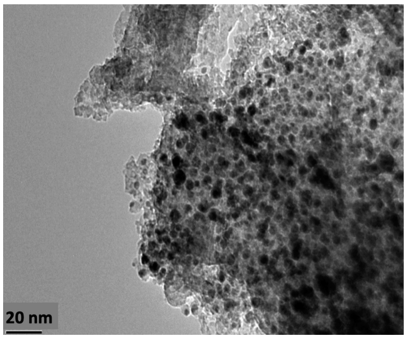

Figure 1. TEM image of the Au/HT-4:1 sample.

The X-ray diffraction (XRD) analysis of Au/HT-4:1 (Figure 2) allowed identifying the presence of two phases: MgO (periclase) and $Mg_6Al_2CO_3(OH)_{16}{\cdot}4H_2O$ (HT). Gold was not observed because of the low metal content (less than 2 wt %), the small size, and the high dispersion of Au NPs. The XRD patterns presented typical diffraction peaks of HT rehydrated because of the Au NP immobilization protocol described below.[15] However, for Au/HT-1:1 and Au/HT-1:5 (not shown), no HT structure was formed, only the presence of Al_2O_3 and MgO was identified. This result is consistent with the study of Cavani *et al.*[16] In fact, with respect to the atomic contents of the ideal HT structure, the molar ratio of M^{2+}/M^{3+} has to be varied between 4:1 and 2:1.[16] HT-1:1 and HT-1:5 were prepared to test the effect of less-basic supports on the reaction.

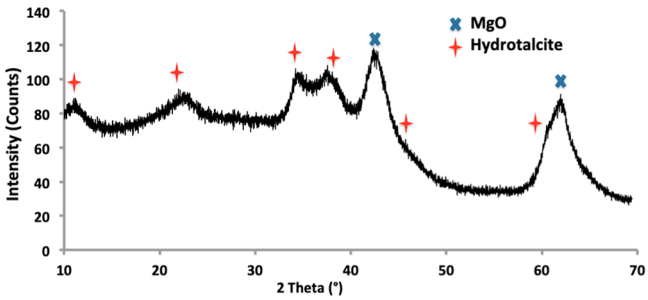

Figure 2. XRD pattern of the Au/HT-4:1 sample.

Concerning the textural properties, it can be seen from Table 2 that Brunauer, Emmett, and Teller (BET) surface areas vary between 111 and 207 $m^2{\cdot}g^{-1}$ and they increase with the Al amount in the support. The same observation is made for the pore volume that doubles from 0.24 to 0.41−0.45 $mL{\cdot}g^{-1}$ when the amount of Al is incremented in HT (Table 2). The pore size is found to be homogeneous between 8 and 10 nm for the 4 supports.

Table 2. BET Surface Area, Pore Volume, and Pore Size of the Supports

Mg/Al (molar ratio)	S_{BET} $m^2{\cdot}g^{-1}$	pore volume $mL{\cdot}g^{-1}$	pore size nm
HT-4:1	111.4	0.24	8.6
HT-2:1	180.4	0.45	9.9
HT-1:1	179.9	0.44	9.9
HT-1:5	206.8	0.41	8.0

Catalytic Tests. In order to determine the best reaction conditions (to be further studied by Raman spectroscopy), four preliminary catalytic tests were carried out under different conditions for the four catalysts having different Mg/Al molar ratios in their support. Results for conversion and selectivity are shown in Figure 3. The carbon balance (CB) was also calculated. It was constant for all catalysts and under all conditions, varying between 86 and 92%. This low CB could be explained by the formation of humins, on the catalyst surface, which results from condensation reactions.[1,17] The only product detected by high-performance liquid chromatography (HPLC) and Raman spectroscopy in the liquid phase after the reaction was furoic acid.

https://dx.doi.org/10.1021/acsomega.0c00091
ACS Omega 2020, 5, 14283−14290

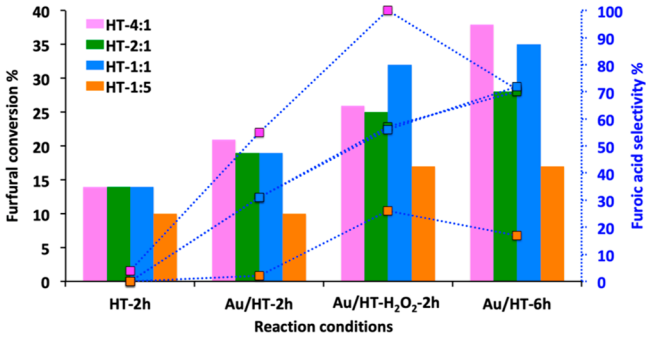

Figure 3. Conversion (histograms) and selectivity (dots) for the preliminary catalytic tests for furfural oxidation using the multireactor (MR) at 90 °C, atmospheric pressure, and a stirring of 600 rpm as fixed conditions. For HT-2 h: bare supports with different Mg/Al ratios (2 h of the reaction time); for Au/HT-2 h and Au/HT-6 h: gold-supported catalysts for 2 and 6 h of the reaction times, respectively; for Au/HT-H_2O_2-2 h, the same conditions as for Au/HT-2 h but with H_2O_2 in the reaction medium (furfural/Au = 100 and furfural/H_2O_2 = 4 in mol).

The first tests were carried out using the 4 different bare HT supports, for 2 h (Figure 3). This series of reaction was named (HT-2 h) where HT stands for the HT support and 2 h stands for the reaction time. For HT-2 h, the conversion is only related to furfural degradation. As a matter of fact, no furoic acid was detected (selectivity = 0) meaning that the presence of Au on the catalyst is absolutely necessary for initiating the furfural oxidation to furoic acid. This result is in agreement with the work reported by Davis *et al.*, which stated that the oxidation reaction occurs on the surface of the gold particles.[18]

Then, the gold-supported catalysts were used with a furfural/Au ratio of 100 but without any oxidant addition. Two series of tests were performed for 2 h (Au/HT-2 h) and 6 h of the reaction time (Au/HT-6 h) using the four Au-based catalysts supported on HTs with different Mg/Al ratios. All catalysts for Au/HT-2 h have shown low conversion and selectivity when compared to the results obtained for the test performed for 6 h under the same reaction conditions (Figure 3). This result indicates that the oxidation reaction took place with only the dissolved O_2 (without the need of O_2 bubbling). Furthermore, these 2 series of tests reflect that the oxidation reaction duration considerably influences the catalytic performance (slow kinetics of the reaction).

Besides, a comparative test was performed under the same conditions as those used for Au/HT-2 h but by adding H_2O_2 to the reaction medium (molar ratio of furfural/H_2O_2 = 4; 3.15 mM of H_2O_2). The conversion and the selectivity obtained for the Au/HT-H_2O_2-2 h tests were significantly increased when compared to the previous test results obtained without H_2O_2 (Figure 3). This demonstrates that the use of H_2O_2 significantly enhances the kinetics of the reaction. This result is consistent with the previous results reported by Comotti *et al.*, which demonstrated that when H_2O_2 is used at a concentration between 10^{-2} and 10^{-1} M, it allows a higher turnover frequency for the oxidation of glucose using a gold catalyst.[13] For this test, the selectivity has reached 100% for Au/HT-4:1.

We should note that the highest conversion of Au/HT-1:1 (condition Au/HT-H_2O_2-2 h) can be related to the high amount of gold immobilized on the catalyst, as shown by ICP characterization. The catalyst Au/HT-1:5 has the highest amount of gold but at the same time the most acid support[17] reflecting the lowest conversion and selectivity.

Finally, the most efficient catalyst was Au/HT-4:1, which has a low amount of Al in its support. The acid−base properties of HTs of different molar ratios undoubtedly affect the catalytic activity.

In conclusion, for the mechanistic study, the Au/HT-4:1 was chosen as the catalyst, using H_2O_2, and at least 6 h of the reaction time.

Raman Study. The Raman scattering light is specific to the analyzed compound and is capable of distinguishing the variation of functionalities that allowed here to follow the oxidation of furfural to furoic acid. This makes it a very useful technique for mechanistic studies. The Raman study enabled us to probe and identify the formation of products in the reaction medium based on their unique fingerprint spectra.

Before setting up the reaction, it was necessary to establish the unique vibrational spectrum for furfural and furoic acid. First, the required concentration level of furfural to get the optimal and distinguished signal was determined by analyzing several concentrations. By using the multipass device, the Raman signal can be detected when the furfural concentration is superior to 12 mmol·L^{-1}. A 64 mmol·L^{-1} solution of furfural dissolved in water was analyzed in order to get a better band resolution (Figure S1). As can be seen in Figure 4, the spectrum obtained experimentally is the same as the one previously reported by Wan *et al.*[19] The details of the vibration can be found in Table 4.

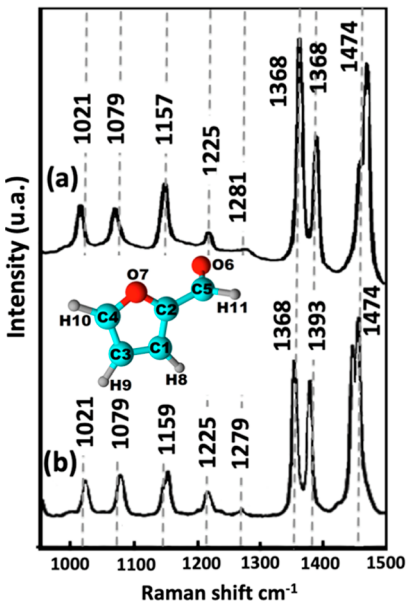

Figure 4. Furfural Raman spectra (a) this work (b) obtained by Wan *et al.* (Adapted in part with permission from [Wan *et al.* **2017**, 7(8), 210, Nanomaterials]. Copyright [2017] [MDPI]).

In Figure 4, only a part of the furfural spectrum (1000−1500 cm^{-1} Raman shift) is presented to compare with the furoic spectrum in the same range. The whole spectrum (500−1500 cm^{-1} Raman shift) is shown in the Supporting Information with the associated vibrational mode (Figure S2). As can be observed, the vibration modes at 1368, 1393, and 1474 (double band) cm^{-1} are the principal bands in the spectrum. Three bands (1021, 1079, and 1157 cm^{-1}), less intense than those above-mentioned, constitute also the fingerprint

https://dx.doi.org/10.1021/acsomega.0c00091
ACS Omega 2020, 5, 14283−14290

spectrum of furfural. These bands arise from the different vibration modes as assigned in Table 3.[19]

Table 3. Raman Vibration Mode Assignments of Furfural Molecules and Comparison with the Literature (Wan *et al.*)

Raman shift (cm^{-1})			
this work	Wan *et al.* 2017	vibrational plane	vibrational mode
1021	1021	in plane	C2−C5−O6−H11; C3−C4−H10−O7 symmetric bend; C2−C1−C3 stretch
1079	1079	in plane	C1−C2−C5−H11; C2−C5−O6−H11 symmetric bend; C1−C2−O7−C4 stretch
1157	1159	in plane	C1−C2−C5−H11 sway; H8−C1−C2−O7−C4 stretch
1225	1225	in plane	C3−C4−H10−O7; C1−C2−C5−H11 asynchronous sway; C2−C1−C3 stretch
1281	1279	in plane	H8−C1−C3−H9; H8−C1−C2−O7−C4 asynchronous stretch; C2−C1−C3 stretch
1368	1368	in plane	H9−C3−C4−H10; C1−C2−C5−H11 synchronous sway
1393	1393	in plane	H8−C1−C3−H9; H8−C1−C2−O7−C4 asymmetric stretch; C2−C1−C3 stretch; H9−C3−C4−H10 sway; C2−C5−O6−H11 sway
1474	1474	in plane	synchronous stretch; H9−C3−C4−H10; C1−C2−C5−H11 asynchronous sway

Furthermore, the furoic acid spectrum was also obtained by analyzing a 64 $mmol{\cdot}L^{-1}$ solution diluted in water. Actually, the use of the multipass cell holder allowed enhancing the Raman signal and detecting the furoic acid at 12 $mmol{\cdot}L^{-1}$ where, for conventional Raman, 200−300 $mmol{\cdot}L^{-1}$ are required.[20]

Each vibration of furoic acid was analyzed and compared to the spectrum reported by Bismondo *et al.*[20] A small shift in the bands values (around 11 cm^{-1} on average for the 8 bands) is observed between the two spectra (Table 4) but the

Table 4. Comparison of Raman Spectral Bands Obtained in This Work and those obtained by Bismondo *et al.*

Raman shift (cm^{-1})		
this work	Bismondo *et al.* 2017	difference
1006	1020	14
1068	1079	11
1122	1132	10
1183	1190	7
1219	1234	15
1287	1298	11
1374	1385	11
1468	1479	10

fingerprints of both spectra were identical. This difference in the band position might be related to the purification of furoic acid by re-crystallization from water/methanol[21] reported by Bismondo *et al.*; whereas for this study, the furoic acid was used without any purification.

The furoic acid spectrum is presented in Figure 5 in the same range as that of furfural (900−1600 cm^{-1} Raman shift). The whole spectrum (900−1800 cm^{-1} Raman shift) is shown in the Supporting Information (Figure S3). There is a predominant band on this spectrum at 1468 cm^{-1} Raman shift. Four other bands at 1011, 1068, 1122, and 1374 cm^{-1}

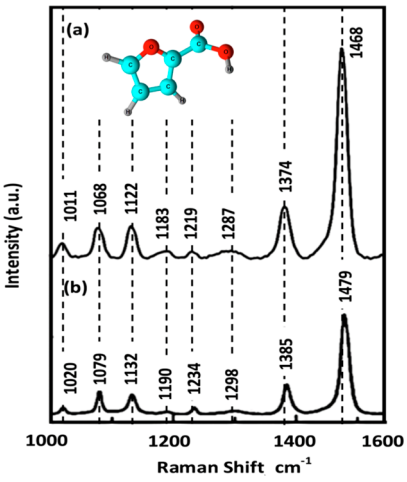

Figure 5. Furoic acid Raman spectra (a) this work (b) obtained by Bismondo *et al.* (Adapted in part with permission from [Bismondo *et al.* **2003**, 469−474, Dalton Transactions]. Copyright [2003] [Royal Society of Chemistry]).

Raman shifts characterize the furoic acid spectrum. These bands can be assigned to the ring vibrations, C−H deformation in plane, and C−OH stretching vibrations.[22]

Mechanism Study. *Raman.* For the mechanistic study in MR, the oxidation of furfural using the Au/HT-4:1 catalyst (furfural/Au = 100) in the presence of H_2O_2 (furfural/H_2O_2 = 4) gives a maximum conversion of 55% after 10 h of the reaction. In order to further increase the furfural conversion (95%), a test was performed using a screening pressure reactor (SPR) system, for 2 h, with the same amounts of the Au/HT-4:1 catalyst, furfural/Au = 100, and furfural/H_2O_2 = 4 in a reactor volume of 6 mL at 90 °C but under 15 bar of air. Figure 6 shows the Raman spectra of the reaction medium obtained from the SPR reactors and the MR at different

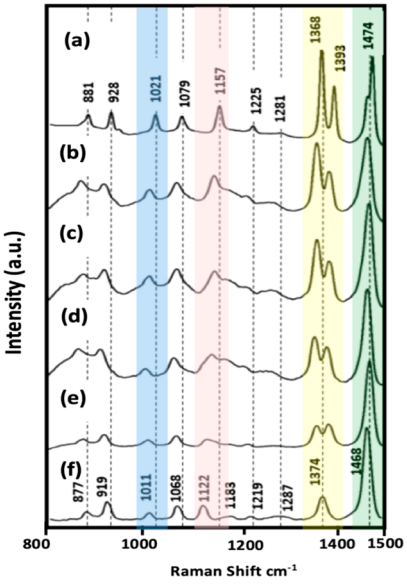

Figure 6. Evolution of the Raman spectra during the progressive conversion of furfural to furoic acid. Spectra (a) furfural at t_0; (b) t = 10 min (12% conversion in MR), (c) t = 270 min (32% conversion in MR), (d) t = 600 min (55% conversion in MR), (e) ≈95% furfural conversion in SPR, and (f) furoic acid.

https://dx.doi.org/10.1021/acsomega.0c00091
ACS Omega 2020, 5, 14283−14290

reaction times. Two band shifts were observed during the course of the reaction: the first one in the blue zone (between 950 and 1150 cm^{-1}) and the second one in the pink zone (between 1100 and 1150 cm^{-1}). Both shifts correspond to the progressive consumption of furfural and concomitant formation of furoic acid: shift of the band 1021 cm^{-1} (furfural) to 1011 cm^{-1} (furoic acid) and shift of the band at 1157 cm^{-1} (furfural) to 1122 cm^{-1} (furoic acid), respectively (Figure 6). Moreover, two bands of the furfural spectrum at 1474 cm^{-1} (green zone) were transformed into one principal band at 1468 cm^{-1}, which is characteristic of the furoic acid spectrum. The double and the most intense bands of furfural in the zone 1360−1400 cm^{-1} (yellow zone) show a decrease of their intensities but did not fully merge to form one single band of furoic acid at 1374 cm^{-1} (Figure 6e). This can be explained by the analysis of a reaction medium at 95% of furfural conversion in SPR experiment that differs from the analysis of a pure furoic acid solution (Figure 6f).

All the above-mentioned band shifts and transformations correspond undoubtedly to the evolution of the principal bands of furfural (an aldehyde) to the ones of furoic acid (described in Figures 4 and 5). No vibration corresponding to other chemical intermediates or products obtained from furfural ring opening was observed in the spectra related to the Raman analysis of the reaction medium. This result shows a direct route of furfural oxidation to furoic acid. Raman spectroscopy coupled to the multipass cell holder has shown to be an efficient tool for monitoring the reaction and is able to give insights into the oxidation mechanism. Furthermore, this Raman evolution was also confirmed by the HPLC analysis because furfural and furoic acids were the only compounds detected on the chromatogram.

ICP Leaching and the HPLC Results. The ICP analysis of the reaction media showed only the presence of Mg (Au and Al were not detected). Hence, Mg has leached progressively with time in the MR solutions (up to 22%).

The furfural conversion to furoic acid results obtained from the HPLC analysis of the reaction medium were then correlated with the leaching results and reaction time. This result is presented as a contour plot and is made using the Minitab software. This graph shows the relationship between one response (*e.g.*, furfural conversion) and two variables (*e.g.*, Mg leaching and the reaction time).

The contour plot shows very clearly that the more the Mg leached within time the higher the conversion of furfural to furoic acid is (Figure 7—dark green zone). The maximum conversion using the MR was 55% after 10 h of the reaction and 22% of Mg leaching.

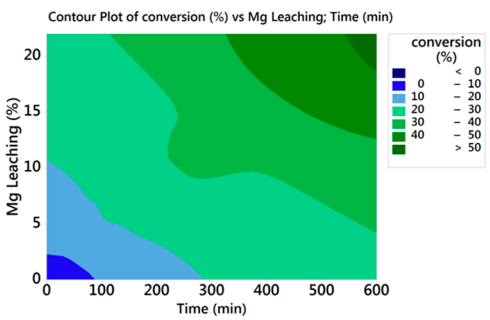

Figure 7. Contour plot of furfural conversion (%) *vs* Mg leaching (%) and the reaction time (min).

It is well known that MgO is poorly soluble in water (86 mg·L^{-1} at 30 °C).[12] The solubility of MgO depends on the pH medium. It has been found that the Mg leaches in the aqueous solution from the basic support when no base is used.[12] In this study, MgO has partially leached from the HT support and it is first hydrated in the aqueous solution forming $Mg(OH)_2$. The dissolution of $Mg(OH)_2$ plays a key role and brings Mg^{2+} and OH^- to the reaction medium according to eq 1

$$Mg(OH)_2 \rightleftarrows 2OH^- + Mg^{2+} \quad (1)$$

The initial pH of the solution containing furfural and H_2O_2 was measured to be 3.6. The measured pH for all MR solutions was around 7.5 because of the presence of $Mg(OH)_2$, even if no additional base was added to the reaction solution. Thus, the dissolved OH^- ions can increase the pH of the solution and act to maintain the neutrality of the reaction medium when furoic acid was produced.[12] The furoic acid formed during the reaction shifts the equilibrium of eq 1 to more dissolved $Mg(OH)_2$. Note that the pH measurement of a furoic acid solution in water was 2.5.

Oxidation Mechanism. Gathering all the information from the preliminary catalytic tests, the Raman study, the HPLC, and ICP analyses (Mg leaching), a mechanism of the oxidation of furfural on gold NPs deposited on a HT support can be proposed.

Raman has shown clearly the evolution of furfural to furoic acid without any intermediate (no ring cleavage nor undesired byproducts). This straight oxidation of an aldehyde to an acid over gold NPs immobilized on HT is discussed in the following.

The mechanism described below is related to the medium conditions (leaching of the basic HT support), the use of H_2O_2 as a reagent, and the gold NPs.

Medium Role. When Mg has leached into the reaction medium, the hydroxide ions released in the solution initiate the reaction by deprotonation of furfural to form an anion (eq 2). This is also supported by the leaching results. In fact, the more the Mg leaches, the more OH^- are present in the solution and the more the catalytic activity increases.

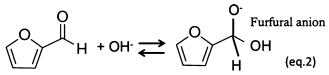

Role of Dissolved O_2. As it was observed in the preliminary tests Au/HT-2 h and Au/HT-6 h (no H_2O_2 and no O_2 bubbling), the catalyst has shown a conversion between 20 and 38%. This can be explained by the study of Zope *et al.* which demonstrates that dissolved molecular oxygen participates indirectly in the catalytic cycle by generating hydroxide ions via the catalytic decomposition of the peroxide intermediate (eqs 3−5).[23]

$$O_2^* + H_2O^* \rightarrow OOH^* + HO^* \quad (3)$$

$$OOH^* + H_2O \rightarrow H_2O_2^* + HO^* \quad (4)$$

$$HO^* + e^- \leftarrow\rightarrow HO^- + * \quad (5)$$

*—metal surface.

Role of H_2O_2. The relatively high concentration of H_2O_2 (3.15 mM) used as a reagent allows increasing the kinetics of the oxidation reaction. It was demonstrated in the preliminary tests that Au/HT-H_2O_2-2 h was more active than Au/HT-2 h where no H_2O_2 was added in the reaction medium. This can be explained by the dissociation of H_2O_2 to form hydroxide

https://dx.doi.org/10.1021/acsomega.0c00091
ACS Omega 2020, 5, 14283−14290

ions on the surface of gold NPs (eqs 4 and 5). The oxidation with H_2O_2 is hence indirect as it regenerates hydroxide ions.

Role of Au NPs. This step is related to the Au-based catalyst where the adsorption and further oxidation of the furfural anion occur. The following mechanism can be proposed (eq 6). The furfural anion forms an electron-rich gold species at the Au NP surface.

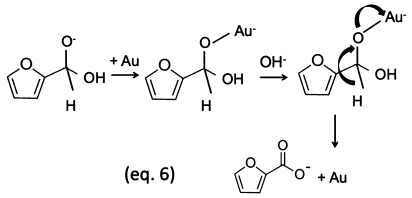

As above-mentioned, when no gold was present in the reaction medium, the formation of furoic acid did not occur. This strongly indicates that the intermediate furfural anion can only adsorb on the gold surface. In the presence of OH ions, the β-hybrid elimination occurs. The formed furoic acid desorbs from the surface regenerating the gold active species.

CONCLUSIONS

In this paper, Raman spectroscopy was used to follow and observe the dynamic functional changes during the oxidation of furfural to furoic acid without the need for sophisticated equipment. The use of a multipass cell holder allowed enhancing the weak Raman scattering and enabled the detection of tens of mmol·L^{-1} of furoic acid. Conventional Raman would allow detection of hundreds of mmol·L^{-1} instead. Also, the laser beam would always be focused on the cell (no further adjustments are required), which is very convenient from the usability standpoint. The compilation of the Raman spectra acquired from different reactors has proved the usefulness of this tool for mechanistic studies. In this study, the Raman spectral evolution has shown a straight pathway for furfural oxidation. Because of raising of the signal and its ease-of-use, the Raman spectroscopy technique associated with the multipass cell holder can be used as an effective tool for monitoring of product reaction evolution over time for any aqueous and environmentally friendly reactions of molecules having polarizable bonds.

Taking advantage of the different information from catalytic tests, vibrational information obtained on the surface of the catalyst, and of the leaching results, a mechanism was proposed for the furfural oxidation in the presence of H_2O_2 as the reagent. The OH ions resulting from $Mg(OH)_2$ leaching guarantee the neutrality of the medium and initiate the oxidation reaction by furfural dehydrogenation. The catalytic tests have shown that even without bubbling O_2 in the reactor, the oxidation took place on the gold NPs (slow kinetics). H_2O_2 enhances the oxidation kinetics by its decomposition on the catalytic surface, via the regeneration of OH ions.

EXPERIMENTAL SECTION

Catalyst Synthesis. $Mg(NO_3)_2{\cdot}6H_2O$, $Al(NO_3)_3{\cdot}9H_2O$, $Na_2CO_3{\cdot}10\ H_2O$, $NaBH_4$, $HAuCl_4{\cdot}3H_2O$ 30 wt % in HCl, polyvinyl alcohol (PVA), furfural, furoic acid (>99%), and H_2O_2 35 wt % in H_2O were all provided by Sigma-Aldrich and used as received without further purification.

Support Synthesis. The four HT supports were prepared by co-precipitating an aqueous solution of Mg and Al salts with different Mg/Al molar ratios (4:1; 2:1; 1:1, and 1:5) with a highly basic carbonate solution.[24] First, a solution of $Mg(NO_3)_2{\cdot}6H_2O$ and $Al(NO_3)_3{\cdot}9H_2O$ dissolved in deionized H_2O (solution 1) was prepared according to the desired Mg/Al molar ratio. The second solution containing the appropriate amount of Na_2CO_3 was added, drop by drop, to solution 1 so that the final Al/CO_3^{2-} molar ratio becomes equal to 2. The pH was then adjusted to 10.5 ± 0.1 with a solution of NaOH (1 M) and the resulting solution was heated for 1 h at 55 °C ± 0.3 under constant stirring. The suspension obtained was then filtered and the recovered solid was washed with warm distilled water. The final solid was dried overnight at 70 °C in an oven and then ground using a mortar. To transform HTs into oxides, the samples were calcined at 500 °C for 3 h under static air with a temperature ramp of 5 °C·min^{-1}.

Gold Deposition on HTs. Au on HT (Au/HT) catalysts were prepared by the sol immobilization method, using polyvinylalcohol (PVA) as a stabilizing ligand and $NaBH_4$ as a reductant.[25] First, a 2 wt % solution of PVA (1200 μL) in distilled water (200 mL) was prepared. After a complete solubilization of PVA, the solution was added to an aqueous solution of $HAuCl_4{\cdot}3H_2O$ (84.3 μL; 5×10^{-4} mol·L^{-1}) under vigorous stirring. A fresh $NaBH_4$ solution (0.1 mol·L^{-1}) was prepared (in order to get a molar ratio $Au/NaBH_4$ of 1:5) and then added to form the metallic sol. The color of the sol was deep purple. After 30 min of sol generation, the gold NPs were immobilized by adding the different HT supports under vigorous stirring. The amount of support was calculated to give a final loading of 2 wt % of gold. After 2 h, the slurry was filtered, the solid was washed with warm water and ethanol and further dried in an oven at 100 °C for 1 h under static air.

Catalyst Characterization. *X-ray Diffraction.* Powder XRD patterns were obtained using a Bruker D8 ADVANCE powder X-ray diffractometer equipped with a Cu Kα_1 radiation source (λ = 0.1538 nm) operating at 40 kV and 40 mA and a 1D Lynx eye detector. The intensity data were collected over a 2θ range of 10−70° with a 0.014° step size using a time counter of 0.1 s per point. Crystalline phases were identified by comparison with the reference data from the Powder Diffractometer Files (PDF) of the ICDD database (International Center for Diffraction Data).

Inductively Coupled Plasma−Optical Emission Spectroscopy. The elemental analyses of the solid samples were performed on a 720-ES ICP−optical emission spectrometer (OES) from Agilent equipped with a coupled charged detector (CCD). The quantification of the metal contents in the catalysts was made based on the analysis of the certified standard solutions. Prior to analysis, powder samples were dissolved using *aqua regia* (HNO_3/HCl) (1:3; v/v) at 110 °C for 2 h in an automated digester Vulcan 42 S (Questron Technologies/HORIBA Jobin Yvon). After the reaction, the medium was also analyzed by ICP to evaluate the leaching of Mg, Al, and Au.

Brunauer, Emmettm and Teller Analysis. Measurements of specific surface areas and porosities of the catalysts were made by nitrogen adsorption/desorption at −196 °C on a TriStar II Plus analyzer from Micromeritics. Prior to analysis, the catalysts were heated up to 75 °C for 3 h and then heated again up to 150 °C for 4 h under vacuum. To determine the total surface area, the BET model was used. The pore volume was also calculated using the Barrett−Joyner−Halenda method.

Transmission Electron Microscopy. TEM analysis was performed using a TEM/scanning TEM FEI TECNAI F20

https://dx.doi.org/10.1021/acsomega.0c00091
ACS Omega 2020, 5, 14283−14290

microscope combined with an energy dispersive X-ray spectrometer at 200 keV. Samples were dispersed in ethanol and left for 10 min in the ultrasonic bath before analysis. For calculating the average gold NP size, the diameters of a minimum of 100 particles were measured from TEM images.

Catalyst Test and HPLC Analysis. *Multi-Reactors.* The catalytic tests were performed using a MR system from Radleys Tech that allows running up to 11 parallel reactions and one blank test at the same time (Figure S4). Each reactor has a capacity of 8 mL and operates under atmospheric pressure (temperature of the reflux fixed at 10 °C). The reactor is equipped with an adjustable mechanical stirrer, as well as a heating system that can heat up to 220 °C. This MR was used for the preliminary catalyst tests to determine the best reaction conditions before studying the mechanism. Four reaction conditions were tested and described in Figure 3.

The MR was also used to perform the mechanistic study via the study of the influence of the time of the reaction on the composition of the reaction medium.

Screening Pressure Reactor. The SPR from Unchained Labs is a MR system that allows conducting 24 parallel tests under high pressure and temperature (same conditions for all the reactors) conditions. Each reactor has a capacity of 6 mL. The SPR can work up to 450 °C and 50 bar for a wide variety of gas. This catalytic test was used to push the furfural conversion to higher values that cannot be reached in the MR system.

High-Performance Liquid Chromatograph. For the analysis of the products of the reaction, an HPLC from Shimadzu was used. The column was a Synergi Hydro-RP (100 × 2.0 mm) with a particle size of 2.5 μm and a pore size of 100 Å. The analysis was conducted under isocratic conditions (T = 30 °C and 210 bar) using 0.5% v/v CHCOOH in H_2O as the mobile phase. The detection was carried out with an UV detector set at 253 nm. The analysis time was 20 min to separate all the compounds (furfural and furoic acid).

Yield, conversion, selectivity, and CB calculations can be found in the Supporting Information.

Raman. The Raman spectra were recorded on a Xplora Raman confocal microscope from HORIBA Jobin Yvon. A 638 nm diode laser was used to excite the samples through a macrodevice connected to a multipass cell holder. A quartz cell from Hellma Analytics was used (Figure 8). The use of the multipass cell holder allows producing a more intense Raman spectrum because of (i) the beam that is reflected 3 times before reaching the detector thus enhancing the intensity, (ii) the spatial resolution of the transparent liquid solution (the volume of sample excited by the electromagnetic radiation) for a macro is greater than the one for a conventional Raman objective, and (iii) the focus for 10 min on a steady sample (Figure S1).

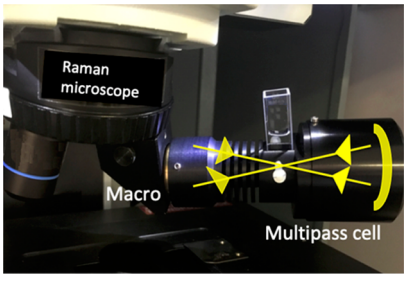

Figure 8. Multipass cell holder with a quartz cell containing the reaction medium.

The Raman signal collected in the backscattering mode was dispersed in the built-in spectrograph by a 1200 g/mm grating and detected by a CCD cooled with a Peltier. The Raman-scattered light was collected in the spectral range 500−1800 cm^{-1}. The spectra were treated using the LabSpec 6 software.

Mechanistic Study by Raman, ICP, and HPLC. To study the mechanism, a unique solution was prepared using 0.01 g of the Au/HT-4:1 catalyst, 101 μL furfural (molar ratio furfural/Au = 100), 27 μL H_2O_2 (molar ratio furfural/H_2O_2 = 4), and 96 mL of H_2O. The reaction was carried out in the MR system with different reaction times for each reactor. To do so, 8 mL of the previous solution was initially placed in six parallel reactors of the MR. Each reactor corresponded to a given reaction time: 10, 90, 150, 270, 520, and 600 min, respectively. T0, corresponding to the beginning of the reaction was also analyzed. After the reaction, the solutions obtained from the different reactors, named T10, T90, T150, T270, T520, and T600, were filtered and placed in the quartz cell for Raman analysis (Figure 8). They were probed one by one using the multipass cell holder.

Each solution was also analyzed by ICP to determine any Mg, Al, or Au leaching. The percentage of Mg leached was quantified according to the initial concentration of Mg in the catalyst before the reaction and those found in the medium according to the following formula

$$\%\ \text{Mg leached} = [\text{MgO}]_{\text{exp}}/[\text{MgO}]_0$$

where $[\text{MgO}]_0$ is calculated for 0.01 g of the catalyst and a ratio of Mg/Al = 4:1 and a volume of 8 mL, $[\text{MgO}]_{\text{exp}}$ is obtained directly by analyzing the reaction medium by ICP.

Furthermore, the reaction medium was also analyzed by HPLC for quantification of the furfural and furoic acid contents and hence calculations of the yield, selectivity, and conversion (an example of calculation can be found in the Supporting Information).

■ ASSOCIATED CONTENT

Supporting Information

The Supporting Information is available free of charge at https://pubs.acs.org/doi/10.1021/acsomega.0c00091.

It contains: Figure S1: a comparison of analysis of [furoic acid] = 64 mmol·L^{-1} by the multipass holder and a conventional Raman objective; Calculation of conversion, selectivity, yield, and CB; Figure S2: Full furfural Raman spectra; Figure S3: Full furoic acid Raman spectra; and Figure S4: MR view; Table S1: All Raman vibrations for furfural; and Table S2: comparison of all bands for furoic acid of the Raman spectra with the literature (PDF)

■ AUTHOR INFORMATION

Corresponding Author

Joëlle Thuriot-Roukos − *Univ. Lille, CNRS, Centrale Lille, Univ. Artois, UMR 8181—UCCS—Unité de Catalyse et Chimie du Solide, F-59000 Lille, France;* orcid.org/0000-0003-0490-718X; Email: joelle.thuriot-roukos@univ-lille.fr

https://dx.doi.org/10.1021/acsomega.0c00091
ACS Omega 2020, 5, 14283−14290

Authors

Romaissa Khadraoui − *Univ. Lille, CNRS, Centrale Lille, Univ. Artois, UMR 8181—UCCS—Unité de Catalyse et Chimie du Solide, F-59000 Lille, France*

Sébastien Paul − *Univ. Lille, CNRS, Centrale Lille, Univ. Artois, UMR 8181—UCCS—Unité de Catalyse et Chimie du Solide, F-59000 Lille, France*

Robert Wojcieszak − *Univ. Lille, CNRS, Centrale Lille, Univ. Artois, UMR 8181—UCCS—Unité de Catalyse et Chimie du Solide, F-59000 Lille, France;* orcid.org/0000-0002-8956-5846

Complete contact information is available at: https://pubs.acs.org/10.1021/acsomega.0c00091

Author Contributions

J.T.-R., R.K., S.P., and R.W. contributed equally. The manuscript was written through contributions of all authors. All authors have given approval to the final version of the manuscript.

Notes

The authors declare no competing financial interest.

■ ACKNOWLEDGMENTS

The authors gratefully acknowledge the support of the French National Research Agency (ANR-11-IS09-0003 and ANR-12-BS07-0029). The REALCAT platform is benefiting from a state subsidy administrated by the French National Research Agency (ANR) within the frame of the "Future Investments" program (PIA), with the contractual reference "ANR-11-EQPX-0037". The European Union, through the ERDF funding administered by the Hauts-de-France Region, has cofinanced the platform. Centrale Lille, the CNRS, and Lille University as well as the Centrale Initiatives Foundation are thanked for their financial contributions to the acquisition and implementation of the equipment of the REALCAT platform. Chevreul Institute (FR 2638) and Ministère de l'Enseignement Supérieur et de la Recherche are acknowledged for supporting and funding partially this work.

■ REFERENCES

(1) Wojcieszak, R.; Ferraz, C.; Sha, J.; Houda, S.; Rossi, L.; Paul, S. Advances in Base-Free Oxidation of Bio-Based Compounds on Supported Gold Catalysts. *Catalysts* **2017**, *7*, 352−375.

(2) Guo, T.; Li, X.; Liu, X.; Guo, Y.; Wang, Y. Catalytic Transformation of Lignocellulosic Biomass into Arenes, 5-Hydroxymethylfurfural, and Furfural. *ChemSusChem* **2018**, *11*, 2758−2765.

(3) Mariscal, R.; Maireles-Torres, P.; Ojeda, M.; Sádaba, I.; López Granados, M. Furfural: a renewable and versatile platform molecule for the synthesis of chemicals and fuels. *Energy Environ. Sci.* **2016**, *9*, 1144−1189.

(4) Serrano-Ruiz, J. C.; Luque, R.; Sepúlveda-Escribano, A. Transformations of biomass-derived platform molecules: from high added-value chemicals to fuels via aqueous-phase processing. *Chem. Soc. Rev.* **2011**, *40*, 5266−5281.

(5) Wachs, I. E. *In situ* Raman spectroscopy studies of catalysts. *Top. Catal.* **1999**, *8*, 57−63.

(6) Wachs, I. E.; Roberts, C. A. Monitoring surface metal oxide catalytic active sites with Raman Spectroscopy. *Chem. Soc. Rev.* **2010**, *39*, 5002−5017.

(7) Bumbrah, G. S.; Sharma, R. M. Raman spectroscopy − Basic principle, instrumentation and selected applications for characterization of drugs of abuse. *Egypt. J. Forensic Sci.* **2016**, *6*, 209−215.

(8) Hartman, T.; Wondergem, C. S.; Kumar, N.; van den Berg, A.; Weckhuysen, B. M. Surface- and Tip-enhanced Raman spectroscopy in catalysis. *J. Phys. Chem. Lett.* **2016**, *7*, 1570−1584.

(9) Grabow, K.; Bentrup, U. Homogeneous catalytic processes monitored by combined *in Situ* ATR-IR, UV-Vis and Raman spectroscopy. *ACS Catal.* **2014**, *4*, 2153−2164.

(10) Tinnemans, S. J.; Mesu, J. G.; Kervinen, K.; Visser, T.; Nijhuis, T. A.; Beale, A. M.; Keller, D. E.; van der Eerden, A. M. J.; Weckhuysen, B. M. Combining operando techniques in one spectroscopic-reaction cell: New opportunities for elucidating the active site and related reaction mechanism in catalysis. *Catal. Today* **2006**, *113*, 3−15.

(11) Stavitski, E.; Weckhuysen, B. M. Infrared and Raman imaging of heterogeneous catalysts. *Chem. Soc. Rev.* **2010**, *39*, 4615−4625.

(12) Fu, J.; He, Q.; Miedziak, P. J.; Brett, G. L.; Huang, X.; Pattisson, S.; Douthwaite, M.; Hutchings, G. J. The Role of $Mg(OH)_2$ in the So-Called "Base-Free" Oxidation of Glycerol with AuPd Catalysts. *Chem.—Eur. J.* **2018**, *24*, 2396−2402.

(13) Comotti, M.; Della Pina, C.; Falletta, E.; Rossi, M. Aerobic Oxidation of Glucose with Gold Catalyst :Hydrogen Peroxide as Intermediate and Reagent. *Adv. Synth. Catal.* **2006**, *348*, 313−316.

(14) Alonso-Fagúndez, N.; Agirrezabal-Telleria, I.; Arias, P. L.; Fierro, J. L. G.; Mariscal, R.; Granados, M. L. Aqueous-phase catalytic oxidation of furfural with H_2O_2: high yield of maleic acid by using titanium silicalite-1. *RSC Adv.* **2014**, *4*, 54960−54972.

(15) Abelló, S.; Medina, F.; Tichit, D.; Pérez-Ramírez, J.; Groen, J. C.; Sueiras, J. E.; Salagre, P.; Cesteros, Y. Aldol Condensations Over Reconstructed Mg−Al Hydrotalcites: Structure−Activity Relationships Related to the Rehydration Method. *Chem.—Eur. J.* **2005**, *11*, 728−739.

(16) Cavani, F.; Trifirò, F.; Vaccari, A. Hydrotalcite-type anionic clays : preparation, properties and applications. *Catal. Today* **1991**, *11*, 173−301.

(17) Roselli, A.; Carvalho, Y.; Dumeignil, F.; Cavani, F.; Paul, S.; Wojcieszak, R. Liquid Phase Furfural Oxidation under Uncontrolled pH in Batch and Flow Conditions: The Role of in Situ Formed Base. *Catalysts* **2020**, *10*, 73.

(18) Davis, S. E.; Ide, M. S.; Davis, R. J. Selective oxidation of alcohols and aldehydes over supported metal nanoparticles. *Green Chem.* **2013**, *15*, 17−45.

(19) Wan, F.; Shi, H.; Chen, W.; Gu, Z.; Du, L.; Wang, P.; Wang, J.; Huang, Y. Charge Transfer Effect on Raman and Surface Enhanced Raman Spectroscopy of Furfural Molecules. *Nanomaterials* **2017**, *7*, 210.

(20) Bismondo, A.; Di Bernardo, P.; Zanonato, P.; Jiang, J.; Rao, L. Complexation of thorium (IV) with 2-furoic acid and 2-thenoic acid in aqueous solution. *Dalton Trans.* **2003**, 469−474.

(21) Armarego, W. L. F.; Perrin, D. D. *Purification of Laboratory Chemicals*, 4th ed.; Butterworth-Heinemann: Oxford, 1996.

(22) Magdaline, J. D.; Chithambarathanu, T. Natural bond orbital analysis and vibrational spectroscopic studies of 2-furoic acid using density functional theory. *Indian J. Pure Appl. Phys.* **2012**, *50*, 7−13.

(23) Zope, B. N.; Hibbitts, D. D.; Neurock, M.; Davis, R. J. Reactivity of the Gold/Water Interface during Selective Oxidation Catalysis. *Science* **2010**, *330*, 74−78.

(24) Zhao, R.; Yin, C.; Zhao, H.; Liu, C. Synthesis, characterization, and application of hydotalcites in hydrodesulfurization of FCC gasoline. *Fuel Process. Technol.* **2003**, *81*, 201−209.

(25) Ferraz, C. P.; Garcia, M. A. S.; Teixeira-Neto, É.; Rossi, L. M. Oxidation of benzyl alcohol catalyzed by gold nanoparticles under alkaline conditions: weak vs. strong bases. *RSC Adv.* **2016**, *6*, 25279−25285.